



# Shrinking annuli mechanism and stage-dependent rate capability of thin-layer graphite electrodes for lithium-ion batteries



Michael Heß, Petr Novák\*

Paul Scherrer Institut, Electrochemistry Laboratory, CH-5232 Villigen PSI, Switzerland

## ARTICLE INFO

### Article history:

Received 7 December 2012

Received in revised form 14 May 2013

Accepted 16 May 2013

Available online 23 May 2013

### Keywords:

Lithium-ion battery

Graphite intercalation compounds

Phase separation

Diffusion limitations

Rate capability

## ABSTRACT

The kinetic performance of graphite particles is difficult to deconvolute from half-cell experiments, where the influences of the working electrode porosity and the counter electrode contribute nonlinearly to the electrochemical response. Therefore, thin-layer electrodes of circa  $1\ \mu\text{m}$  thickness were prepared with standard, highly crystalline graphite particles to evaluate their rate capability. The performance was evaluated based on the different stage transitions. We found that the transitions toward the dense stages 1 and 2 with  $\text{LiC}_6$  in-plane density are one of the main rate limitations for charge and discharge. But surprisingly, the transitions toward the dilute stages 2L, 3L, 4L, and 1L progress very fast and can even compensate for the initial diffusion limitations of the dense stage transitions during discharge. We show the existence of a substantial difference between the diffusion coefficients of the liquid-like stages and the dense stages. We also demonstrate that graphite can be charged at a rate of  $\sim 6\ \text{C}$  (10 min) and discharged at  $600\ \text{C}$  (6 s) while maintaining 80% of the total specific charge for particles of  $3.3\ \mu\text{m}$  median diameter. Based on these findings, we propose a shrinking annuli mechanism, which describes the propagation of the different stages in the particle at medium and high rates. Besides the limited applicable overpotential during charge, this mechanism can explain the long-known but as yet unexplained asymmetry between the charge and discharge rate performance of lithium intercalation in graphite.

© 2013 Elsevier Ltd. All rights reserved.

## 1. Introduction

Graphite is one of the most important negative electrode materials used in current lithium-ion batteries due to its very negative open-circuit potential, improved safety compared to metallic lithium and moderate cost. But it has some major drawbacks, such as its moderate specific charge of  $372\ \text{mAh/g}$  and its rather low practical rate capability, which is limited to  $\sim 2\ \text{C}$  for lithiation (charge with respect to a complete battery) and  $20\ \text{C}$  for delithiation (discharge) in standard electrodes [1]. However, recent *ab initio* calculation based on density functional theory (DFT) and Monte Carlo simulations [2] yielded a diffusion coefficient larger than  $D = 2 \times 10^{-8}\ \text{cm}^2/\text{s}$  for the diffusion of lithium in dense stages 1 and 2 in the presence of many vacancies. But the diffusion coefficient decreases to  $5 \times 10^{-9}\ \text{cm}^2/\text{s}$  for fully lithiated stages 1 and 2 due to a low number of vacancies for Li hopping [2]. Similar results have been found experimentally by Levi et al. [3], who determined the diffusion coefficient by applying the potentiometric intermittent titration technique at  $60^\circ\text{C}$  using the Cottrell equation. These experiments revealed highly fluctuating diffusion coefficients of approximately  $5 \times 10^{-9}\ \text{cm}^2/\text{s}$  for the transitions involving dense

stages 1 and 2 that drop sharply to  $10^{-10}\ \text{cm}^2/\text{s}$  at the end of each phase transition. For the liquid-like phases, i.e., stage 2L, 3L, 4L, and 1L, the diffusion coefficient was determined to be approximately  $1\text{--}5 \times 10^{-8}\ \text{cm}^2/\text{s}$ , dropping to a minimum of  $10^{-9}\ \text{cm}^2/\text{s}$  at the end of each phase transition [3]. This suggests a difference in the lithium diffusion coefficients of a factor of 10 for the liquid-like stages compared to the dense stages with  $\text{LiC}_6$  in-plane density. In any case, from both the *ab initio* calculation [2] and the experiment [3], one would expect the rate capability of graphite to be higher than  $\sim 2\ \text{C}$  for charge and  $20\ \text{C}$  for discharge [1] for particles in the micrometer range.

It is known that the performance of graphite electrodes depends significantly on the electrode preparation, due to its influence on the porosity, the tortuosity, and the overall electronic conductivity of the graphite network [1,4]. To characterize the properties of graphite particles themselves, however, it is necessary to avoid parasitic effects, such as electrolyte diffusion limitation within the porous electrode, electronic conductivity limitations, and the influence of the counter electrode. It has been shown for electrochemical impedance spectroscopy and cyclic voltammetry that thin layers of graphite can be used to separate the different electrochemical influences in a graphite electrode [5]. Therefore, we prepared thin-layer electrodes of graphite flakes in this work and, thus, aimed at avoiding porosity effects and reducing the active mass and consequently the specific currents applied to the electrolyte and the

\* Corresponding author. Tel.: +41 56 310 2457; fax: +41 56 310 4415.  
E-mail address: [petr.novak@psi.ch](mailto:petr.novak@psi.ch) (P. Novák).

## Nomenclature

### List of symbols

$A$	area, $\text{m}^2$
$a_i$	interfacial specific area, $\text{m}^2$
$c_e$	concentration of salt in electrolyte, $\text{mol m}^{-3}$
$c_0$	concentration of solvent, $\text{mol m}^{-3}$
$D_e, D_s$	diffusion coefficient in electrolyte, $\text{solid m}^2 \text{s}^{-1}$
$f$	activity coefficient, $\text{mol m}^{-3}$
$F$	Faraday's constant, $96,485 \text{ C mol}^{-1}$
$h$	porous electrode thickness, $\text{m}$
$i$	current density, $\text{A m}^{-2}$
$i_0$	exchange current density, $\text{A m}^{-2}$
$I$	superficial current density, $\text{A m}^{-2}$
$J$	diffusion flux, $\text{mol m}^{-2} \text{s}^{-1}$
$m$	mass, $\text{g}$
OF	oxidation factor
$Q$	charge, $\text{mAh}$
$r$	particle radius, $\text{m}$
$R$	universal gas constant, $8.3143 \text{ J mol}^{-1} \text{ K}^{-1}$
$R_0$	contact resistance, $\Omega$
$R_{\text{SEI}}$	resistance of solid–electrolyte interphase, $\Omega$
$S$	dimensionless number for diffusion influence
$t^0$	transference number
$T$	temperature, $\text{K}$
$U_{\text{OCP}}$	open-circuit potential, $\text{V}$
$z$	number of electrons
$\alpha_{a,c}$	transfer coefficient, anodic/cathodic
$\varepsilon$	porosity of electrode
$\eta$	surface overpotential, $\text{V}$
$\kappa$	conductivity of electrolyte, $\text{S m}^{-1}$
$\sigma$	conductivity of solid matrix, $\text{S m}^{-1}$
$\Phi$	electrical potential, $\text{V}$

### Subscripts

e	electrolyte in the separator
s	solid phase
n	normal direction
TL	thin layer

lithium counter electrode. These thin layers consist of 2–3 flat graphite flakes stacked above one another (approximately  $1 \mu\text{m}$  thickness) and directly reflect the particles' properties.

To understand the kinetics of the lithiation and delithiation of graphite, we separated the results into the different stage transitions. The stages of the lithium–graphite binary system at room temperature are depicted in Fig. 1. The stages are named by the ordering of the lithium ions in every  $n$ -th interslab. Additionally, the letter L indicates liquid-like, disordered lithium ordering in every  $n$ -th interslab. Starting from pure graphite, 4–7% of lithium with respect to  $\text{LiC}_6$  (state-of-charge (SOC) of 100%) can be intercalated into stage 1L (solid–solution of lithium in graphite) [6], where every layer is filled with lithium ions in a liquid-like manner, i.e., without any in-plane order. Then, a phase separation occurs to form stage 4L from stage 1L, with every fourth interslab filled in a liquid-like manner. A debate about the transitions between stages 4L, 3L, and 2L is still ongoing. X-ray diffraction experiments (XRD) indicate that the  $c$ -axis parameter shifts continuously with increasing lithium intercalation [6] without a clear sign of phase separation. By contrast, minor peaks appear in the cyclic voltammetry, indicating stage transitions [5]. However, it is known that stage 3L consists of disordered lithium ions in every third interslab. The next stage transition occurs from stage 2L, with every second interslab filled without any in-plane order, to the ordered dense stage 2, with  $\text{LiC}_6$

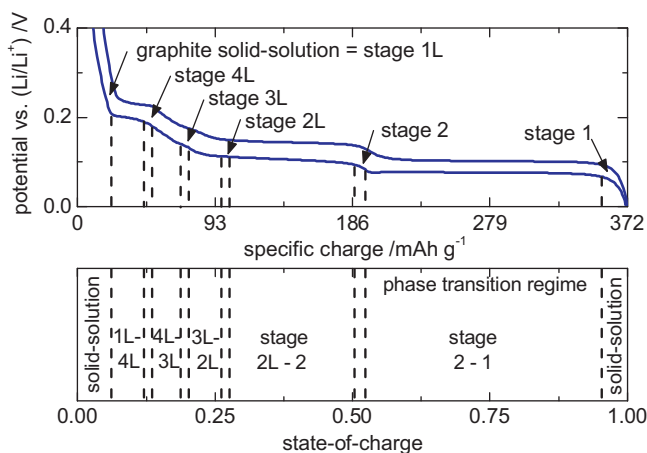


Fig. 1. Different stages and stage transitions of graphite during lithium intercalation, dashed lines indicate solid–solution regime of each phase at room temperature with coexistence regime between pure phases.

in-plane ordering in every other interslab [7]. Finally, a phase separation from stage 2 to stage 1 occurs, forming a  $\text{LiC}_6$  structure in every interslab. In dense stages 1 and 2, the lithium ions align in straight columns, unlike all other alkali and earth alkali metals [8]. The intercalation kinetics of graphite can be understood in terms of these stage transitions.

In the first section of this article, the kinetics of a porous electrode will be discussed based on the work of Doyle et al. [9]. Their equation system will be used to identify the main influences governing the thin-layer half-cell electrode. In the second section, we will use the thin-layer model electrode to investigate the rate capability of graphite considering the side reactions occurring in these electrodes. In the last section, a model is proposed to explain the asymmetry of the rate capability between charge and discharge.

## 2. Experimental

Graphite SFG6 (TIMCAL) was used for all experiments. This sample has a specific surface area of approximately  $17.1 \text{ m}^2/\text{g}$  (from BET) and 50% and 90% of the graphite particles are smaller than 3.3 and  $6 \mu\text{m}$  along the  $a$  and  $b$ -axis, respectively [10]. The dimension of the flakes along the  $c$ -axis of the SFG6 graphite sample is approximately  $0.4 \mu\text{m}$ , as estimated from the scanning electron microscopy image shown in Fig. 2a. This kind of graphite consists of highly crystalline graphite flakes with a primary crystallite size along the  $a$  and  $b$ -axis of  $\sim 30 \text{ nm}$  ( $L_a$ ) and  $\sim 60 \text{ nm}$  along the  $c$ -axis ( $L_c$ ), as determined from XRD [10]. Slurries of graphite (90 wt%) and PVDF binder (Kynar Flex, 10 wt%) in  $N$ -methyl-pyrrolidone (NMP)

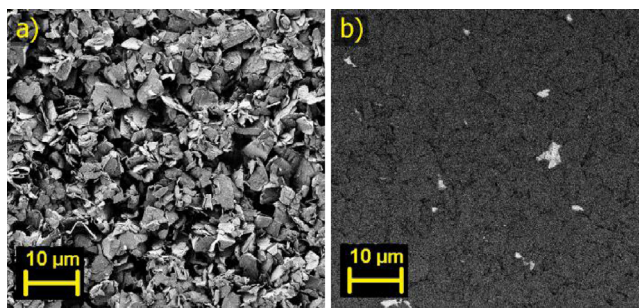


Fig. 2. Scanning electron microscope images of thin-layer electrodes of SFG6 graphite; (a) secondary electron detector, (b) electron backscattering detector (graphite appears black and copper appears gray).

Download English Version:

<https://daneshyari.com/en/article/6616855>

Download Persian Version:

<https://daneshyari.com/article/6616855>

[Daneshyari.com](https://daneshyari.com)